OBSERVATIONAL CHARACTERIZATION OF THE DOWNWARD ATMOSPHERIC LONGWAVE RADIATION AT THE SURFACE IN THE CITY OF SÃO PAULO

Eduardo Barbaro, Amauri P. Oliveira, Jacyra Soares, Georgia Codato, Maurício J. Ferreira

Group of Micrometeorology, Department of Atmospheric Sciences,

Institute of Astronomy, Geophysics and Atmospheric Sciences,

University of São Paulo, São Paulo, SP, Brazil.

Primož Mlakar, Marija Z. Božnar,

MEIS d.o.o., Mali Vrh pri Šmarju, Slovenia.

and

João F. Escobedo

Department of Natural Resources, School of Agronomic Sciences,

State University of São Paulo, Botucatu, SP, Brazil.

Corresponding author address:

Amauri Oliveira, Micrometeorology Group

Atmospheric Sciences Dept., IAG-USP

Rua do Matão 1226, São Paulo, SP, Brazil, 05508-090

e-mail: apdolive@usp.br

ABSTRACT

This work describes the seasonal and diurnal variations of downward longwave atmospheric irradiance (*LW*) at the surface in the city of São Paulo, Brazil, using 5-minute average values of *LW*, air temperature, relative humidity and solar radiation observed continuous and simultaneously from 1997 to 2006 on a micrometeorological platform, located at the top of four-store building. An objective procedure, including 2-step filtering and dome emission effect correction, was used to evaluate the quality of the 9-year long *LW* dataset. The comparison between *LW* values observed and yield by the *SRB* Project shows spatial and temporal agreement, indicating that monthly and annual average values of *LW* observed in one point of the city of São Paulo can be used as representative of the entire Metropolitan Region of São Paulo. The maximum monthly averaged value of *LW* is observed during summer (389 ±14 W m^{-2}; January) and the minimum during winter (332 ±12 W m^{-2}; July). The effective emissivity follows the *LW* and shows a maximum in summer (0.907±0.032; January) and a minimum in winter (0.818±0.029; June). The mean cloud effect, identified objectively comparing the monthly averaged values of *LW* during clear sky days and all sky conditions, intensified the monthly average *LW* in about 32.0±3.5 W m^{-2} and the atmospheric effective emissivity in about 0.088±0.024. In August, the driest month of the year in São Paulo, the diurnal evolution of *LW* shows a minimum (325±11 W m^{-2}) at 09 local time and a maximum (345 ±12 W m^{-2}) at 18 local time that lags behind in 4 hours the maximum diurnal variation of the screen temperature. The diurnal evolution of effective emissivity shows a minimum (0.781 ±0.027) during daytime and a maximum (0.842±0.030) during nighttime. The diurnal evolution of all sky condition and clear sky days differences in the effective emissivity remain relatively constant (7±1%) indicating that clouds do not change the emissivity diurnal pattern. The relationship between effective emissivity and screen air temperature and between effective emissivity and water vapor is rather complex. During night, when the planetary boundary layer is shallower, the effective emissivity can be estimated by screen parameters. During the day, the relationship between effective emissivity and screen parameters varies from place to place and depends on the planetary boundary layer process. Because the empirical expressions do not contain enough information about the diurnal variation of the vertical stratification of air temperature and moisture in São Paulo they are likely to fail in reproduce the diurnal variation of the surface emissivity. The most accurate way to estimate *LW* for clear sky conditions in São Paulo is using an expression derived from a purely empirical approach.

Key Words: Downward atmospheric longwave radiation, Metropolitan Region of São Paulo, Satellite Observations, Empirical expressions.

1. Introduction

Downward atmospheric longwave radiation fluxes at the surface (*LW*) play an important role in the air-surface interaction. It can be estimated from (i) radiative transfer models; (ii) empirical expressions and (iii) observations. Despite the good performance, radiative transfer models are difficult to use regularly because they require information about the atmospheric thermodynamic state, aerosol load and composition, vertical distribution of moisture and other greenhouse gases (Ellingson et al. 1991; Dutton 1993; Mlawer et al. 1997; Turner et al. 2004). Comparatively, empirical expressions are easy to apply but they are limited to the conditions of theirs derivations and they also require long-term measurements of radiation fluxes, screen air temperature and air water vapor pressure to be validated for a particular site and season (Prata 1996; Crawford and Duchon 1999; Iziomon et al. 2003; Finch and Best 2004, Bilbao and de Miguel 2007; Flerchinger et al. 2009). Downward longwave radiation at the surface estimated from satellite data requires a combination of radiative transfer modeling, empirical expression applications and *in situ* observations (Garratt 2001; Gupta et al. 1992; Iziomon et al. 2003). Direct observations of *LW* are more precise when compared to the other techniques, but for heterogeneous surfaces they are less representative. According to Albrecht and Cox (1977), pyrgeometers require special care due to the fact that the sensor emission (dome and case) has to be taken into consideration explicitly. Several authors introduced, following Albrecht and Cox (1977) work, some refinement to the dome emission correction improving the accuracy of *LW* measurements with commercially available pyrgeometers reducing the error to below 5%, e.g. Fairall et al. (1998), Payne and Anderson (1999), Philipona et al. (2001), Burns et al. (2003), Marty et al. (2003) and Philipona et al. (2004).

Despite the importance, measurements of *LW* at the surface are very rare in Brazil (Duarte et al. 2006; Oliveira et al. 2006). The Group of Micrometeorology of the University of São Paulo started measuring downward longwave radiation at the surface in the City of São Paulo

(Fig. 1) in October 1997 (Oliveira et al. 2006). In this work, 5-minute averaged measurements of *LW* carried out in the city of São Paulo continuously during 9 years, from 1997 to 2006, will be used to characterize the seasonal variation of *LW* at the surface.

The city of São Paulo, with about 11 million inhabitants, together with 38 other smaller cities, forms the Metropolitan Region of São Paulo (*MRSP*). This region, located about 60 km far from the Atlantic Ocean (Fig. 1b), is occupied by 20.5 million inhabitants and has approximately 7 million vehicles. The *MRSP* has an area of 8,051 km^2 and it is the largest urban area in South America and one of the 10 largest in the world. Even though pollution is the most dramatic environmental problem in the *MRSP*, the assessment of the pollution impact on the local climate is still incipient. There is evidence that pollution in São Paulo has altered the local climate by affecting the diurnal variation of diffuse, direct and global solar irradiance components at the surface locally (Oliveira et al. 2002a) and in regional scale (Codato et al. 2008).

Regional patterns of clouds and moisture play also an important role in the solar radiation features in São Paulo. For instance, the comparison between the seasonal variations of daily and hourly values of global and diffuse solar radiation at surface in the city of São Paulo and rural area in the vicinity, has indicated that São Paulo receives, during clear sky days, 7.8 % less of global irradiance in August and 5.1 % less in June than rural areas at the same latitude and altitude. On the other hand, São Paulo receives, during clear sky days, more 3.6 % of diffuse irradiance in August and 15.6 % more in June than rural areas. The seasonal variation of the diurnal cycle confirmed these differences and indicated that they are more pronounced during afternoon time (Codato et al. 2008). The regional differences in solar radiation at the surface are mainly related to the distance from the Atlantic Ocean, that in turns determine the spatial and temporal distribution of moisture and clouds in São Paulo. The systematic penetration of sea breeze during the afternoon in São Paulo brings moisture and maritime

aerosol increasing the solar radiation scattering and reducing the intensity of the direct component of solar radiation at the surface (Codato et al. 2008).

The main objective of this work is to characterize the seasonal variation of *LW* in the city of São Paulo using the available measurements of longwave radiation and other meteorological parameters like air temperature, air relative humidity and global and diffuse radiations measured at the Institute of Astronomy, Geophysics and Atmospheric Sciences, (*IAG*), located at the University of São Paulo campus, in the west portion of city of São Paulo (Oliveira et al. 2002a). Here, a detailed analysis will be carried in *LW* dataset in order to guaranty its quality by removing errors associate to sensor malfunctioning and dome emission effects. In the particular case of pyrgeometer used in São Paulo the malfunctioning is detected and removed objectively by a 2-step filtering and the dome emission effect is removed using neural network technique proposed by Oliveira et al (2006) and heat balance equation originally proposed by Albrecht and Cox (1977) and refined by several authors. The corresponding values of global solar radiation, air temperature and relative humidity are also removed from the dataset to guarantee the consistence of dataset. In the same direction, comparison between *in situ* observation and satellite estimates of *LW* are used to investigate whether only one point of observation (*IAG*) may be used to represent the *LW* atmospheric emission in the entire *MRSP* and the existing gaps in the dataset compromise the temporal representativeness of *LW* measurements carried out in São Paulo.

In the second part of this work the seasonal and diurnal variations of *LW* at the surface in São Paulo is addressed and special attention is given to the role played by clouds. Here, the seasonal and diurnal variations of *LW* are analyzed by comparing the effective emissivity for clear sky and all sky conditions (Malek 1997; Long and Turner 2008). A general approach concerning validation, use and development of empirical expressions to estimate *LW* at the

surface for clear sky days is proposed that may settle down the question concerning the criteria of choice and how to incorporate local characteristics in formulations.

This is accomplished by showing that empirical expressions available in the literature can not reproduce the diurnal variation of the effective emissivity of São Paulo, because they are based on screen temperature and water vapor measurements that do not convey enough information about the local diurnal variation of thermal and moisture stratification. In the diurnal time scale, the contribution of lower layers of the atmosphere to *LW* at the surface is strongly dependent on the diurnal evolution of the Planetary Boundary Layer (*PBL*) that, in turn, depends on the surface exchange process. The discrepancy associated to the misrepresentation of the *PBL* is particularly important during daytime in areas of complex land used like urban regions. The simplest way to overcome all these difficulties is by developing a pure empirical approach.

A description of the data used in this work, as well the methodology to remove glitches from *LW* observations and improve their precision using heat balance equation and neural network technique to correct dome emission effect are described in section 2. This section also includes an evaluation of the spatial and temporal representativeness of *LW* measurements by comparing monthly and annual values of *LW* observed in one point and estimated from satellite. The characterizations of the seasonal and diurnal variations of *LW* in São Paulo are addressed in sections 3 and 4, respectively. In these sections the seasonal and diurnal variation of *LW* are analyzed comparing the effective emissivity for clear sky and all sky conditions. The use and development of empirical expressions for estimate *LW* are addressed in section 5 and the relevant findings of this work are summarized in section 6.

2. Data description

All meteorological measurements were taken on a micrometeorological platform located at the top of the building of the Institute of Astronomy, Geophysics and Atmospheric Sciences (*IAG*) of the University of São Paulo, in the western portion of the city of São Paulo, Brazil (Fig. 1), at 744 m above mean sea level ($23^0$33'35"S; $46^0$43'55"W). The sensors and measurement periods are indicated in Table 1. The measurements were taken with a sampling frequency of 0.2 Hz and stored as 5-minute averages in a datalogger 21X from Campbell Inc. Simultaneously and with the same sampling frequency it is also measured (i) global solar radiation, (ii) air temperature (iii) and air relative humidity at the surface level.

The *LW* has been regularly measured in São Paulo city since October 1997 using a pyrgeometer model *PIR* from Eppley Lab. Inc. This instrument performs hemispherical, broadband, infrared radiative flux measurements, using thermopile temperature difference. Its composite transmission window associated to the silicon dome properties is 4-50 μm (Philipona et al. 1995; Ji and Tsay 2000). The pyrgeometer model *PIR* comes with a battery-powered resistance circuitry that provides voltages that allow estimating the radiative flux contribution due to the case and dome temperatures simultaneously to thermopile output. However, extra channels to record in the datalogger both case and dome temperatures became available only in 15 October 2003. From this date on, dome and case temperatures were used to correct dome emission effects on the pyrgeometer measurements as described in section 2b. Prior this date, the pyrgeometer *PIR* measured only the thermopile output and neural network procedure was applied to correct the dome effect as described in section 2c.

A pyranometer, model 8-48, built by Eppley Lab. Inc., measured global solar irradiance. A pyranometer model *PSP*, built by Eppley Lab. Inc. and coupled to a shadow ring device measured diffuse solar irradiance (Oliveira et al. 2002b). These sensors have been periodically calibrated using as secondary standard a spectral precision pyranometer model *PSP*, from Eppley Lab. Inc. The calibration consists of running, at least once a year, side-by-

side, both pyranometers continuously during 2 to 7 days (Oliveira et al. 2002a). A new calibration factor is evaluated by comparing output voltages measured by pyranometers and using, as reference, the calibration factor of pyranometer model *PSP*.

Air temperature and air relative humidity were estimated using a pair of thermistor and capacitive sensors from Vaisala. According to the manufacturer, the air temperature and relative humidity are measured with an accuracy of 0.1 ^{o}C and 2% respectively, for a range of temperature 0 and 40 ^{o}C and 10 to 90%.

Sensors measuring *LW*, global and diffuse solar radiation, air temperature, relative humidity and rain are set up 1.5 meters above the surface located at the top of a four-store building. Therefore, in this work, screen air temperature and water vapor represent the data of 1.5 meters above the roof surface. The *LW* measurements were carried without any horizontal obstruction, so that they can be considered as valid for sky view factor equal to 1 (Jonsson et al. 2006).

a. Data quality control

Fig. 2a-c shows the raw data from 1997 to 2006 of shortwave radiation (Fig. 2a), air temperature (Fig. 2b) and *LW* (Fig. 2c). In order to filter the raw data, a 2-step filter was applied. The first step is intended to removes only the physically inconsistent values, i.e. the larger signal incursions in *LW* (Fig.2c), using as thresholds 0 W m^{-2} and 1000 W m^{-2}, and removing *LW* values outside these limits. This procedure removes only the *LW* data related to connection malfunctioning or pyrgeometer battery failure. It was removed simultaneously all parameters even when the glitches happened only in one of them to make the dataset consistent. This procedure is responsible for removing most part of doubtful data.

However, there were time periods when the pyrgeometer was not totally working because of the battery malfunctioning (initial stages) and the resulting effect on the *LW* data was more

difficult to identify since the pyrgeometer was not totally shut down. Other common problem is related to the accumulation of rain and dust over the sensor. To attenuate the contamination of these problems, a second step consisting into remove *LW* values located out of two standard deviation interval centered in the mean value (362 ± 64 W m^{-2}) was applied to the data inspection procedure. The corresponding values of global solar radiation (*SW*), air temperature and air relative humidity were also removed from the dataset when *LW* was removed in the previous steps.

To guarantee representativeness in description of the diurnal cycle, data corresponding to an entire day were removed when 4 or more 5-minute average values were missing. The filtered dataset is indicated in Fig. 2d-f. The filtered dataset (Fig. 2d-f) consists of 64% (602,134 values for each parameter) of the raw data (Fig. 2a-c). The *LW* filtered is displayed in Fig. 2f.

b. Pyrgeometer dome emission effect correction using heat balance equation

The atmospheric longwave emission measured by a pyrgeometer model *PIR*, manufactured by Eppley Lab. Inc., can be estimated considering the heat balance equation originally proposed by Albrecht and Cox (1977) and modified by Fairall et al. (1998) and Payne and Anderson (1999).

$$LW_{CORRECTED} = \frac{\Delta V}{s_0} + \sigma T_C^4 + B\sigma\left(T_C^4 - T_D^4\right) \quad (1)$$

Where $LW_{CORRECTED}$ is the corrected value of longwave radiation, ΔV is the thermopile voltage, σ is the Stefan-Boltzmann constant, T_C and T_D are, respectively, the case and dome temperatures, s_0 and B are calibration factors dependent of the sensor direct calibration. The calibration factor s_0 is known as the fundamental radiometer sensitivity constant and it

depends on the thermopile thermal conductivity, paint emissivity, sensor temperature and dome characteristic represented by factor *B*. The factor *B*, known as dome factor, represents the ratio of dome emittance to dome transmittance.

According to Fairall et al. (1998), considering the third term on the right side of expression (1) reduces the error to 3.5%. In this work, simultaneous measurements of *LW*, T_C and T_D were available after 15 October 2003. In the case of the pyrgeometer used here (model PIR and serial number 28594F3), the value of s_0, provided by the manufacturer, is equal to 3.63±0.04 μV $W^{-1}m^2$ and the *B* value is equal to 3.5. Details about the derivation of s_0 and *B* for most of the pyrgeometers available commercially can be founded in Albrecht and Cox (1977), Philipona et al. (1995), Fairall et al. (1998), Payne and Anderson (1999) and Burns et al. (2003). The value of *B* used here (3.5) was proposed by Fairall et al. (1998) after analyzing several different calibrations of pyrgeometers model *PIR*.

After 15 October 2003 $LW_{CORRECTED}$ was estimated using expression (1). Before this date, *LW* was estimated based on the neural network (*NN*) technique (LW_{NN}) procedure developed by Oliveira et al. (2006) and described in the next section.

c. Pyrgeometer dome emission effect correction using neural network

The neural network applied in this case used a training set (learning and optimization dataset) employing data measured during the years 2004 (7 days) and 2005 (2 days) corresponding to 2,578 observations. The optimization dataset was based on randomly selected 10% of patterns from the original training set and it was used during the training process to periodically test the Multilayer Perceptron Neural Network (*MLP*) performance as the "unknown" dataset to determine its generalization capabilities (Mlakar and Božnar 1997; Gardner 1998; Soares et al. 2004). The final network was the one that gave the smallest error on the optimization dataset and not on the training set. These 9 days were chosen based on

heuristic method, from patterns defined as dry, wet, cold, cloudy and clear sky days. Based on analysis performed previously by Oliveira et al. (2006), the most relevant parameters for the construction of the dome effect correction were: observed longwave radiation, global solar radiation, air temperature and relative humidity.

According to Oliveira et al. (2006), the standard back propagation algorithm with a learning rate 0.3 and momentum 0.5 provided a quick and effective learning of the chosen neural network type – *MLP*. It should be emphasized that the *MLP* used here is a 3-layer Perceptron with logistic (sigmoid) activation function and back propagation learning algorithm, (Božnar and Mlakar 1998, 2002). The first *MLP* layer contains 4 neurons, the second layer 50 neurons and third layer 1 neuron.

The time variation of the difference between *LW* corrected - prior 15 October 2003 by the NN and after this date by expression (1) - and *LW* filtered ($LW_{FILTERED}$) is indicated in the Fig. 3a. As indicated by vertical black line in Fig. 3a there is no apparent discontinuity in the series after the *NN* correction. Most of the rectification was negative, confirming that the adjustment applied to pyrgeometer measurements are due to the dome heating (daytime solar radiation). The determination coefficient (R^2) between LW_{NN} and $LW_{CORRECTED}$ of 99.1% indicates a good matching between both dataset, for the year of 2004 (Fig. 3b). The 7 days randomly selected in 2004 used in the training of the neural network was not included in the dispersion diagram of Fig. 3b. One plausible reason for LW_{NN} to overestimate $LW_{CORRECTED}$ for low values of atmospheric emission (Fig. 3b) is the fact that *NN* corrections applied here does not consider the wind like a predictor. According to Pérez and Allados-Arboledas (1999) under natural or forced ventilation T_C and T_D gets closer and the correction using expression (1) reduces. The *NN* corrections do not recognize this pattern because it is not present in the predictors set. Another possibility is that to correct *LW* measurements under clear sky conditions (small *LW* values) would be necessary to incorporate information about thermal and moisture

stratification from deeper layers, whose signature is not present in the data set used to train the *NN* algorithm (screen air temperature and relative humidity, global solar radiation. The problem concerning the lack of correlation between *LW* and screen air temperature and vapor pressure will be addressed in the section 4 in the context of effective broadband emissivity of the atmosphere of city of São Paulo, however it is important to bring up this question here because this lack of correlation may have an important impact on the methodology of correction of dome emission effects.

d. Representativeness of LW measurements

Hereafter, the *LW* measurements resulting of the application of 2-step data filtering and dome emission effect correction (using NN technique before and expression (1) after 15 October 2003) will be refereed only as *LW* measurements.

To evaluate the spatial and temporal representativeness of *LW* measurements, two comparisons were performed considering monthly and annual averaged values of *LW* measured at *IAG* and estimated from satellite data of the Surface Radiation Budget (*SRB*) Project, LW_{SRB}, of the Atmospheric Science Data Center from *NASA* (Figs. 4 and 5).

The *SRB* estimates are derived from the vertical structure of the atmosphere and surface properties datasets combined with satellite observations and radiation transfer equations for short and longwave radiations provide several surface and atmospheric parameters with spatial resolution of 1 degree of latitude by 1 degree of longitude, with 3-hourly time resolution (Darnell et al. 1983; Gupta et al. 1992; Gupta et al. 1993; Gupta et al. 1999; Wilber et al. 2006). According to Gupta et al (1999), among short and longwave radiation components yield by the *SRB* project, the *LW* estimates is the one that shows the largest level of disagreement with respect to *in situ* observations and general circulation models simulations, with an overall uncertainty of 15 W m^{-2} for monthly average values.

A two-sample test for variance (Snedecor and Cochran, 1989; Wilks, 2006) was performed using the *LW* estimated from *SRB* (1998-2004) to check the spatial representativeness of the seasonal variation of *LW* observed in São Paulo (1997-2006). This test indicates for monthly values of *LW* and LW_{SRB}, an *F-value* of 1.22 and *P-value* of 0.75, therefore it is possible to assume, with 5% level, that the variances are not significantly different. The statistical parameters, mean bias error (*MBE*) and root mean square error (*RMSE*) were also used to quantify the compatibility of the *LW* and LW_{SRB} magnitudes. The *MBE* indicates the magnitude of the mean deviation and provides information about the long term performance. A small absolute value of *MBE* is a necessary condition for a good performance; however it does not suffice because an overestimation can superpose an underestimation. Positive *MBE* indicates that the observations overestimate *SRB* and vice-versa. The normalized root mean square error (*RMSE*) indicates how well, in percent terms, the *SRB* values approach the observations, providing information about short-term performance, considering that *RMSE* value permits a comparison term by term of standard deviation between datasets. In general, small *RMSE* are associated with good estimates (Targino and Soares 2002).

In the specific case of São Paulo, a negative mean *MBE* (-12.9 W m^{-2}) and a small normalized mean *RMSE* (3.6%) indicate that the *SRB* values slightly overestimates the observed values (Table 2). One possible reason for this discrepancy is that LW_{SRB} depends on the cloud base height estimates, which according to Gupta et al. (1992) is not precisely estimated in the *SRB* dataset. The monthly variation of the *MBE* (Fig. 4, Table 2) indicates that the LW_{SRB} values slightly overestimate the *LW* during the whole year, presenting larger values in May and smaller in October. The *MBE* values, however, are similar to the errors involved in the *LW* (3.5%*)* and LW_{SRB} (15 W m^{-2}*)*.Thus, from the climate point of view the measurements carried out in the *IAG* can be considered representative of the entire *MRSP*

describing the seasonal variation of *LW* above the urban canopy (Fig. 1c). The consistency between observation and *SRB* estimates indicates that the 2-step filtering procedure carried out in the observations (section 2a), where 36 % of the original dataset was removed, did not introduce any significant bias in the seasonal representation of *LW* in São Paulo.

The annual *LW* measurements started in first of October of 1997. Therefore, excluding 1997 year, the maximum difference between *LW* annual values is around 16 W m^{-2} (*LW* annual mean is maximum in 2001 and minimum in 2006). Considering that observations in 2006 finished on August, it is expected that the *LW* mean in 2006 and the *LW* annual difference appear slightly underestimated and overestimated respectively (Table 3).

The number of observations during summer (December, January and February) and winter (June, July and August) is not the same (Table 3). The largest fractions of valid observations occurred during winter months, between 1998 and 2006, (except in 1999 and 2001); however, considering the number of observations in summer period (robustness) and the heterogeneity in the data distribution, it can be assumed that both summer and winter are well represented in the dataset.

The annual observations are validated using the LW_{SRB} values because the *SRB* dataset presents almost no gaps during the investigated period.

The test for variance of annual values of *LW* and LW_{SRB} indicates an *F-value* of 3.98 and a *P-value* of 0.11, allowing assuming that, at 5% level, the two variances are not significantly different. The mean *MBE* (-14.7 W m^{-2}) and mean *RMSE* (4.1%) values indicate that the *SRB* data slightly overestimate the observed values (Table 3).

The *MBE* annual values show a small time variation with LW_{SRB} always overestimating the observed *LW* (Table 3 and Fig. 5). The only exception is year 2000 when a large amount of data was removed in the data inspection procedure (section 2a and Figs. 2c and 2f).

In short, from the climate point of view the *LW* measurements carried out in the *IAG* describes the annual variation of longwave radiation in the city of São Paulo. The constancy and consistency presented by the difference bias indicate that *SRB* dataset may be a good indicator of data quality, providing useful information about changes over time in the performance of sensors used in "*in situ*" long time observations.

3. Seasonal variation of *LW* in São Paulo

Considering that the mean annual values of *LW* (Fig. 5) remained practically constant, this work will focus on the description of the seasonal and diurnal variations of *LW* in São Paulo

The city of São Paulo climate - typical of subtropical regions of Brazil - is characterized by a dry winter during June-August and a wet summer during December-March (Oliveira et al. 2003). The minimum values of monthly-averaged daily temperature and relative humidity occur in July and August (16^{o}C and 74%, respectively), and the minimum monthly-accumulated precipitation occurs in August (35 mm). The maximum value of monthly-averaged daily temperature occurs in February (22.5^{o} C) and the maximum value of monthly-averaged daily relative humidity occurs from December through January and from March through April (80%). The seasonal distribution of surface wind speed indicates that the São Paulo urban area is characterized by light winds throughout the year, with intensity varying between 0.5 m s^{-1} (January and May) and 1.5 m s^{-1} (September through October), preferentially from N-NE direction.

The seasonal variation of *LW* values is consistent with the expected for the climate of São Paulo described above. The *LW* maximum during summer (389±14 W m^{-2}, January) is due to the maximum in the temperature, water vapor and cloud activity. The *LW* minimum during winter (332±12 W m^{-2}; July) occurs at the driest and cold period of the year, when there is

little cloud activity (Fig. 4). The effective emissivity follows the *LW* and shows a maximum in summer (0.907±0.032; January) and a minimum in winter (0.818±0.029; June).

The *LW* variations among December, January and February (0.5 W m^{-2}) and June, July and August (1.3 W m^{-2}) months are smaller than the variations among the transition periods (fall, -20.6 W m^{-2} and spring, 10.1 W m^{-2}).

The seasonal variation of monthly average hourly values of *LW* in *MRSP* reflects the combination of local climate patterns of air temperature, moisture and clouds (Fig. 6). The *LW* observed in São Paulo shows a maximum of 389±14 W m^{-2} during summer daytime (January - 11 local time, *LT*) and a minimum of 332±11 W m^{-2} during winter daytime (June - 10 *LT*). The local maximum (*LW* > 330 W m^{-2}) observed in May-June during dawn period may be related to the fog formation. This pattern is not observed during other winter months because the moisture content of atmosphere becomes progressively smaller reaching a minimum in August.

a. Mean cloud effect

Based on Malek (1997) and Long and Turner (2008), a subset of *LW* measurements including only clear sky days was used to investigate the mean cloud effect on the *LW* radiation in São Paulo, comparing the *LW* observed under clear sky with the *LW* considering all sky conditions.

It should be pointed out that when comparing clear days to all days, the cloud effect is not totally isolated because partly cloudy days and clear times are included in the averages. Unfortunately, it was not possible to isolate completely cloud effect because independent information about cloud cover was not available at the site. However, most of the mean cloud

effects identified here will not qualitatively change by using a more precise way to isolate the contribution of clouds.

Following the diurnal variation of global and diffuse solar irradiances at the surface it is possible, by visual inspection, to identify days when the sky was not significantly covered by clouds. Here, a clear sky day was considered when the curves of the diurnal variation of global and diffuse solar irradiances are simultaneously smooth and have a distinct separation early in the morning and come together only at the end of the day. Between 1997 and 2006 it was identified 138 days satisfying the clear sky conditions described above. The monthly frequency distribution of clear sky days over 1997-2006 are indicated in Fig. 7 for São Paulo. The seasonal distribution indicates a maximum frequency during winter and minimum during summer. As expected, the largest number of clear sky days occurs in August, the driest month of the year.

The method to select clear sky days uses global and diffuse radiations at the surface and does not distinguish layers of high clouds. However, according to Dürr and Philipona (2004), the presence of high clouds will not affect *LW* measured at the surface because most of the longwave downward atmospheric emission (90%) comes from the first 1000 meters of the atmosphere.

The seasonal variation of monthly averaged values of *LW*, air temperature, air vapor pressure and atmospheric effective emissivity, considering all days and clear sky days, are indicated in Fig. 8.

The effective emissivity is defined as broadband effective emissivity, $LW/\sigma T^4$, where T is the air temperature measured at screen level varying in most of the cases between 1.5 and 2 meters above the surface (Prata 1996; Niemelä, 2001, Iziomon et al. 2003; Jonsson et al. 2006). The effective emissivity is seen as a bulk atmospheric property that indicates the

capability of lower layers of atmosphere to emit downward longwave radiation at the surface as consequence of theirs composition and thermal stratification (Brunt 1932; Brutsaert 1975; Alados-Arboledas and Jimenez 1988; Malek 1997; Long and Turner 2008; Grobner et al. 2009).

Clear sky averages are statistically significant only between April and September when the number of clear sky days are larger than 5% (Fig. 7). The presence of clouds, in average, increases the *LW* (Fig. 8a), in 32.0±3.5 W m^{-2} (2.76±0.30 MJ m^{-2} day^{-1}). The presence of clouds may also be associated to air temperature about 1.05±0.41 ^{o}C lower (Fig. 8b) and vapor pressure about 1.67±0.35 hPa higher (fig. 8c). The clouds increase also the atmospheric effective emissivity (Fig. 8d). The averaged cloud contribution to clear sky effective emissivity is equal to 0.088±0.024.

4. Diurnal variation of *LW* in São Paulo

Figure 9 considers the observations carried in São Paulo only in August, the month with the largest number of clear sky days, (Fig. 7). When only clear sky days are considered, the diurnal variation of *LW* shows larger amplitude but smaller intensity (Fig. 9a), indicating that the presence of clouds not only increases the intensity of *LW* (325±11 W m^{-2} at 09 *LT* and 345±12 W m^{-2} at 18 *LT*), because clouds emit in the atmospheric window, but also decreases its diurnal cycle amplitude, due to the cloud base temperature in average does not vary much during the day. Air temperature and water vapor differences between all and clear days are concentrated during daytime when clear sky values of air temperature increases and water vapor decreases more than for all sky conditions (Fig. 9b,c).

The differences in the effective emissivity remain relatively constant and equal to 0.060±0.007, or about 7±1% during the entire day (Fig. 9d), indicating that the presence of clouds mainly increases the effective emissivity values but do not alter its pattern.

Changes in air temperature (Fig. 9b) and water vapor (Fig. 9c) patterns, considering all days and clear sky days, seem to not alter the effective emissivity pattern (Fig. 9d). Furthermore, effective emissivity variation is modulated by the water amount variation during the end of convective (15-18 *LT*) and nighttime periods (18-06 *LT*). During the convective period (06-15 *LT*) the effective emissivity seems to change with non-local effects, e.g. erosion of the surface inversion layer temperature and early morning peak in the latent heat flux.

The daytime drops in the effective emissivity (Fig. 9d), observed in both clear sky and all sky conditions, can be explained in terms of day and night contrast of the lower atmosphere stability. During daytime, even in the presence of clouds, the diurnal variation of the convective *PBL* alters the stability in the first 2 km over São Paulo. This effect is a robust feature of the local atmosphere present in both clear sky and all sky. The diurnal variation in the effective emissivity for all sky condition is basically due to the *PBL* effects induced by the presence of 138 clear sky days and a large numbers of clear sky periods in the partially cloudy days existing in dataset. Observational works indicates that the *PBL* height in the city of São Paulo varies from a maximum of 200±100 meters at nighttime to a maximum of 2000±500 meters during daytime (Nair et al. 2004; Marciotto 2009).

According to Grobner et al. (2009), measurements of *LW* at the surface contains enough information about the *PBL* to infer the thermal vertical structure of the lower layers by just comparing broadband *LW* measurements and *LW* in the atmospheric window. Therefore, the effective emissivity represents better than surface parameters the *PBL* upper layers.

The screen vapor pressure and air temperature are equally important in the definition of the diurnal variation of effective emissivity during nighttime because the vertical stratification at nighttime is confined to surface adjacent layers.

As pointed by Alados-Arboledas and Jimenez (1988) the diurnal variation of the effective emissivity should include the time variation of the vertical thermal stratification. The delay between daytime maximum of monthly average temperature (23.2±0.1 ˚C at 18 *LT*) and *LW* (345±12 W m^{-2} at 14 *LT*) is caused by the time taking to erode the surface inversion during the morning (Figs. 9a, b), indicating that the correlation between air temperature at the screen level and *LW* is phased out (4 hours in the case of August).

5. Estimating LW for clear sky conditions in São Paulo

The main objective of this section is to find a simple method to estimate *LW* in clear sky conditions in São Paulo, which could be easily implement in algorithms to evaluate the energy balance at the surface in urban areas (Arnfield and Grimmond 1998; Martilli et al. 2001; Orfelle et al. 2003; Karam et al. 2009).

For better accuracy, the method needs to take into account the effective emissivity dependence on temperature and moisture vertical structures of the shallower layers of the atmosphere that contributes to the most of the *LW* at the surface (Dürr and Philipona 2004).

It was observed in the previous sections that the relationships between effective emissivity (Fig. 9d) and screen air temperature (Fig. 9b) and between effective emissivity and water vapor (Fig. 9c) are rather complex. During night, when the planetary boundary layer is shallower, the effective emissivity can be estimated by screen parameters. During the day, the relationship between effective emissivity and screen parameters is more complex because it varies from place to place and depends on *PBL* process (Alados-Arboledas and Jimenez 1988; Crawford and Duchon 1999; Dürr and Philipona 2004; Long and Turner 2008; Grobner *et al.* 2009).

Following previous authors, e.g. Ellingson et al. (1991), Dutton (1993), Mlawer et al. (1997) and Turner et al. (2004), the most accurate way to estimate *LW* for clear conditions is

using radiative transfer equation (*RTE*); however, the scarcity of appropriate information precludes the use of *RTE* approach. For instance, in the urban area of the city of São Paulo, radiosondes are carried out twice a day and estimating hourly values of *LW* will require value interpolations, which will introduce a large uncertainty in the *LW* estimates.

An alternative to estimate *LW* at the surface for clear sky conditions is using simple empirical expressions (Brunt et al. 1932; Swinbank 1963; Brutsaert 1975; Prata 1996; Dilley and O'Brien 1998; Crawford and Duchon 1999; Niemelä et al. 2001; Iziomon et al. 2003; Finch and Best 2004, Bilbao and de Miguel 2007; Flerchinger et al. 2009).

However, choosing the best expression among the available in the literature is not an easy task, leading to concerns about the criteria of choice, validation procedure and how to incorporate local characteristics in the formulation.

Given the above concerns, it becomes clear that making additional observations to perform *RTE* calculations compete, in terms of difficulty and limitations, with selecting and applying the best empirical expression relative to the desired accuracy applications. Therefore, a more appropriate method to estimate *LW* is using a purely empirical approach (*PEA*), where a nonlinear fit is performed through *LW* values without specifying the relationship between *LW* and screen parameters. The result of this approach is indicated below (expression 2) and it will be shown that this expression performs better than other *LW* empirical expression available in the literature. In addition, the use of the *PEA* methodology implies in a better reproduction of the diurnal variation of the effective emissivity observed in São Paulo.

$$LW = 1827.23 + 31.35\,T_0 - 35.06\,e_0 - 967.82\ln(T_0) - \frac{7725.26}{T_0} + 390.92\sqrt{e_0} + \frac{2372.20}{e_0} \quad (2)$$

where T_0 and e_0 are, respectively, the air temperature (˚C) and vapor pressure (hPa) at the screen level.

Expression (2) was developed using the dataset containing 5-minute averaged values of *LW*, air temperature and water vapor pressure, measured in the city of São Paulo during clear sky days. The dataset was split in two parts (65% and 35%) selected randomly, (Lütkepohl 1993). The largest part was used to develop and the other one to test the expression. The main reason to use the 5-minutes averaged values to develop the *PEA* is the fact that this database can capture most of all the *LW* patterns like hourly and daily and monthly variabilities. The final result is the parameterization that better approximates the *LW* data (R^2=*0.55*).

In the *PEA*, the methodology itself is more important than the resulting expression, because this formulation is valid only to São Paulo. It should be mentioned that the nonlinear fit must be done using *LW* instead of the effective emissivity because, from the mathematical point of view, the diurnal variation of *LW* (Fig. 9a) is more suitable to interpolation than the effective emissivity (Fig. 9d). Considering that *LW* values are necessary, *a priori*, to develop the formulation, satellite data could be used in the case of absence of *in situ* measurements.

To illustrate the performance of expression (2), 6 empirical expressions are used to estimate the *LW* for clear sky days at the surface in São Paulo (Brunt et al. 1932; Swinbank 1963; Brutsaert 1975; Prata 1996; Dilley and O'Brien 1998; Niemelä et al. 2001), using *MBE*, *RMSE* and index of agreement (*d*). The index of agreement, *d,* (Willmott, 1981) varies between 0 and 1 and indicates the level of fitness between estimates and measurements. It can be applied in order to make a cross-comparison between the estimates and the observations (Willmott, 1982). Values of *d* close to 1 indicate a good performance of the estimates with respect to the observations.

$$d = 1 - \frac{\sum_{i=1}^{N} \left(LW_i^{estimates} - LW_i \right)^2}{\sum_{i=1}^{N} \left(\left| LW_i^{estimates} - \overline{LW} \right| + \left| LW_i - \overline{LW} \right| \right)^2} \quad (3)$$

Where $LW^{estimates}$ are the 5-minute average *LW* values estimated by the empirical expressions; $\overline{LW}$ correspond to mean values of observed *LW* values. *N* indicates the number of the data set (602,134 values).

The performance of *LW* expressions can be visualized in Fig. 10. All expressions overestimate the observed *LW* values, presenting a positive *MBE*. In addition, all the expressions perform better during nighttime (Fig 10b) because all of them are sensitive to air temperature and vapor pressure fluctuations, which are more intense through daytime due to the shortwave radiation. Moreover, the *PBL* is shallower during night and the effective emissivity can be better estimated by screen parameters. Another reason for better agreement is the lack of solar heating interference in the pyrgeometer performance. As expected, the *PEA* expression presented the smallest *MBE*, *RMSE* and the biggest *d* (Fig. 10) but it is not very discrepant from Brunt's expression.

However, even the screen temperature near the surface does not totally reflect the thermal structure of the lower layers, slightly overestimating the emission during daytime and underestimating during nighttime (Alados-Arboledas and Jimenez 1988; Dürr and Philipona 2004; Jonsson et al. 2006; Long and Turner 2008). The *PEA* better reproduces the diurnal variation of effective emissivity in the *MRSP* (Fig. 11). A larger degree of discrepancy in the diurnal emissivity pattern was observed for the other 5 expressions (not shown here).

Attempts to calibrate the 6 expressions improved the performance (*MBE*, *RMSE*, *d* and closeness to the diurnal variation of effective emissivity) as expected, but none of them performed better than the *PEA*. Besides, there is no guarantee that expressions with best

results without calibration will provide the best fit after the procedure, bringing up questions relating to the criteria of choice. Moreover, the amount of work used to perform the calibration of one unique expression was equivalent to entire *PEA* procedure, indicating that using available expressions, even when they are calibrated against local data is not the most appropriate way to estimate *LW* under clear sky conditions.

6. Conclusions

The main objective of this work was to characterize the seasonal and diurnal variation of *LW* in the city of São Paulo, using 5-minute averaged measurements of *LW*, global and diffuse solar radiations, air temperature and air relative humidity carried out at the surface continuously during 9 years, from 1997 to 2006.

A 2-step filtering methodology was developed to evaluate the *LW* data consistency observed in São Paulo. This procedure removed about 36% of the *LW* observations due sensor malfunctioning and problems in the data acquisition system. After that, the pyrgeometer dome emission effect was removed of the *LW* filtered dataset, using neural network technique (prior to 15 October 2003) and using heat balance equation (after to 15 October 2003).

Comparison between the *LW* observed in São Paulo and yield by *SRB* Project indicated a good spatial and temporal agreement for the variation of monthly and annual values. The mean *MBE* (-12.9 W m^{-2}) and mean normalized *RMSE* (3.6%) values indicate that the *SRB* data slightly overestimate the observed values for seasonal variation. However, this overestimate is at the same order of the errors associated with measurements and estimates. For annual basis, the *MBE* (-14.7 W m^{-2}) and mean normalized *RMSE* (4.1%) indicate that both observations and *SRB* are compatible from the climatological point of view. In addition, the maximum discrepancy of *LW* among the years is 16 W m^{-2}. Therefore, the existing gaps in the dataset do not compromise the temporal representativeness of *LW* measurements carried

out in São Paulo and one point observation can be used to represent the *LW* atmospheric emission in the entire *MRSP*. These inferences are valid only in the climatological context of monthly and annual means.

The *LW* observed in São Paulo shows a maximum of 398±14 W m^{-2} during summer daytime (January - 11 *LT*) and a minimum of 323±11 W m^{-2} during winter daytime (June - 10 *LT*). The characterizations of seasonal and diurnal variations, based on monthly averaged 5-minute values of *LW*, included an analysis of the mean cloud effect on the effective emissivity. This parameter conveys information about the vertical stratification of temperature and moisture that is not clearly identified only in screen parameters. Following Malek (1997) and Long and Turner (2008), mean cloud effects were successfully identified by comparing the *LW* observed under clear sky with the *LW* considering all sky conditions. Clear sky averages are statistically significant only between April and September when the number of clear sky days are larger than 5%. The largest number of clear sky days occurs in August (138 days in 9 years), the driest month of the year in São Paulo.

The seasonal variation of *LW* in São Paulo indicates that the maximum monthly averaged values of *LW* are observed during summer (389±14 W m^{-2}; January) and the minimum during winter (332±12 W m^{-2}; June). Following the *LW* pattern, the effective emissivity, considering all days, shows a maximum in summer (0.907±0.032; January) and a minimum in winter (0.818±0.029; June). In average, the presence of cloud intensifies the monthly averaged values of *LW* by about 32.0±3.5 W m^{-2} and the effective emissivity at the surface by about 0.088±0.024. The seasonal variation of monthly average hourly values of *LW* in *MRSP* reflects the combination of local climate patterns of air temperature, moisture and clouds.

The diurnal variation of *LW* for clear sky days in August shows larger amplitude but smaller intensity than *LW* for all sky conditions, indicating that the presence of clouds not only increases the intensity of *LW* but also decreases its diurnal cycle amplitude. It was shown

that there is a delay (of 4 hours in case of August) between daytime maximum of monthly average hourly values of *LW* (345±12 W m^{-2} at 18 LT) and screen temperature (23.2±0.1 ^{o}C at 14 LT) caused mainly by the time taking to erode the surface inversion during the morning. The diurnal variations of the effective emissivity show a minimum of 0.781±0.027 (0.720±0.025) during daytime and a maximum of 0.842±0.030 (0.790±0.028) during nighttime for all sky condition (clear sky days). There is no apparent diurnal variation in the difference of the effective emissivity, considering all day and only clear sky conditions, (0.060±0.007) or about 7±1%. Hence, the mean clouds effect increases the amplitude of the effective emissivity but do not alter its diurnal pattern. The effective emissivity diurnal variation is mainly modulated by the water amount variation during the end of convective (15-18 *LT*) and nighttime periods (18-06 *LT*). During the convective period (06-15 *LT*) the effective emissivity responds to the surface inversion layer erosion and the early morning peak in the latent heat flux.

In this work, a traditional approach of applying empirical expressions to estimate diurnal evolution of *LW* in clear days is investigated. The methodology is useful to better characterize the most important patterns of *LW* observations in clear days. It was found that empirical *LW* expressions available in the literature are not able to reproduce the *LW* in São Paulo because they cannot reproduce the diurnal variation of the effective emissivity. The reason for this mismatched is because the empirical *LW* expressions do not convey enough information about the diurnal variation of the thermal and moisture stratification, mainly the daytime *PBL* evolution. The simplest way to improve the *LW* estimates is using purely empirical approach based on *in situ LW* measurements because it can better accounts for the effective emissivity diurnal cycle.

Acknowledgments: We acknowledge financial support provided by *CNPq* (476807/2007-7), *FAPESP* and *CAPES*. The *SRB* data were obtained from the *NASA* Langley Research

Center Atmospheric Science Data Center. We also wish to thank the anonymous reviewers whose comments improved the presentation of this work.

REFERENCES

Alados-Arboledas, L., and J. I. Jimenez, 1988: Day-night differences in the effective emissivity from clear skies. *Bound-Layer Meteor.*, **45**, 93-101.

Albrecht, B. A., and S. K. Cox, 1977: Procedures for improving pyrgeometer performance. *J. Appl. Meteor.,* **16,** 188–197.

Arnfield, A.J., and C.S.B., Grimmond, 1998: An urban canyon energy budget model and its application to urban storage heat flux modeling. *Energy and Building,* **27**, 1-26.

Bilbao, J., and A. H. de Miguel, 2007: Estimation of daylight downward longwave atmospheric irradiance under clear-sky and all-sky conditions. *J. Appl. Meteor. Climatol.*, **4**, 878-889.

Božnar, M., and P. Mlakar, 1998: Improvement of air pollution forecasting models using feature determination and pattern selection strategies. In: *Air pollution modeling and its application XII.* Eds. S.-E. Gryning and N. Chaumerliac. Plenum Press, New York, 725-726.

——, 2002: Use of neural networks in the field of air pollution modeling. In: *Air pollution modeling and its application XV*. Eds. C. Borrego and G. Schayes. Kluwer Academic, New York, 375-383.

Brunt, D., 1932: Notes on radiation in the Atmosphere. *Q. J. R. Meteorol. Soc.* **58**, 389-420.

Brutsaert, W., 1975: On a derivable formula for long-wave radiation from clear skies *Water Resources Research*, **11**, 742-744.

Burns, S. P., J. Sun, A. C. Delany, S. R. Semmer, S. P. Oncley and T. W. Horst, 2003: A field intercomparison technique to improve the relative accuracy of longwave radiation

measurements and an evaluation of CASES-99 pyrgeometer data quality. *J. Atmos. Oceanic Technol*.**, 20**, 348-361.

Codato, G., A. P. Oliveira, J. Soares, J. F. Escobedo, E. N. Gomes and A. D. Pai, 2008: Global and diffuse solar irradiances in urban and rural areas in southeast of Brazil, *Theor. Appl. Climatol.,* **93(1-2)**, 57-73.

Crawford, T. M. and C. E. Duchon, 1999: An Improved Parameterization for Estimating Effective Atmospheric Emissivity for Use in Calculating Daytime Downwelling Longwave Radiation. *J. Appl. Meteor.*, **38**, 474-480.

Darnell, W. L., S. K. Gupta and W. F. Staylor, 1983: Downward longwave radiation at the surface from satellite measurements. *J. Clim. Appl. Meteorol*., **22**, 1956-1960.

Dilley, A. C., and D. M. O'Brien, 1998: Estimating downward clear sky long-wave irradiance at the surface from screen temperature and precipitable water. *Q. J. R. Meteorol. Soc.,* **124**, 1391–1401.

Duarte, H. F., N. L. Dias, and S. R. Maggiotto, 2006: Assessing daytime downward longwave radiation estimates for clear and cloudy skies in Southern Brazil. *Agricultural and Forest Meteorology*, **139**, 171–181

Dutton, E.G., 1993: An extended comparison between LOWTRAN7 computed and observed broadband thermal irradiances: Global extreme and intermediate surface conditions. *J. Atmos. Oceanic Technol.***, 10**, 326-336.

Dürr, B. and R. Philipona, 2004: Automatic cloud amount detection by surface longwave downward radiation measurements. *J. Geophys. Res.*, **109**, D05201, doi: 10.1029/2003JD004182.

Ellingson, R. G., J. Ellis and S. Fels, 1991: Intercomparison of radiation codes used to climate models: Long wave results. *J. Geophys. Res.*, **96**, 8929-8963.

Fairall, C. W., P. O. G. Persson, E. F. Bradley, R. E. Payne and S. P. Anderson, 1998: A new look at calibration and use of Eppley precision infrared radiometers. Part I: Theory and application. *J. Atmos. Oceanic Technol.*, **15**, 1229-1242.

Finch, J. W., and M. J. Best, 2004: The accuracy of downward short- and long-wave radiation at the earth's surface calculated using simple models. *Meteorol. Appl.*, **11**, 33–39.

Flerchinger, G. N., Xaio, W., Marks, D., Sauer, T. J., and Q. Yu, 2009: Comparison of algorithms for incoming atmospheric long-wave radiation. *Water Resources Research*,. **45**, W0342, doi:10. 1029/2008WR007394.

Grobner, J., S. Wacker, L. Vuilleumier, and N. Kampfer, 2009: Effective atmospheric boundary layer temperature from longwave radiation measurements, *J. Geophys. Res.*, **114**, D19116, doi:10.1029/2009JD012274.

Gardner, M. W., and S. R. Dorling, 1998: Artificial neural networks (The multiplayer Perceptron) – A review of applications in the atmospheric sciences. *Atmos. Environ.*, **32(14-15)**, 2627-2636.

Garratt, J. R., 2001: Clear-Sky Longwave Irradiance at the Earth's Surface – Evaluation of Climate Models: *J. Climate,* **14**, 1647-1670.

Gupta, S. K., W. L. Darnell and A. C. Wilber, 1992: A parameterization for longwave surface radiation from satellite data: Recent improvements. *J. Appl. Meteorol*., **31**, 1361-1367.

——, A. C. Wilber, W. L. Darnell and J. T. Suttles, 1993: Longwave surface radiation over the globe from satellite data: An error analysis. *Int. J. Remote Sensing*, **14**, 95-114.

——, N. A. Ritchey, A. C. Wilber, C. H. Whitlock, G. G. Gibson and P. W. Stackhouse, Jr, 1999: A climatology of surface radiation budget derived from satellite data. *J. Climate*, **12**, 2691-2710.

Iziomon, M. G., H. Mayer and A. Matzarakis, 2003: Downward atmospheric longwave radiation under clear and cloudy skies: Measurement and parameterization. *J. Atmos. Solar-Terr. Phys.*, **65**, 1107-1116.

Ji, Q. and S-C. Tsay, 2000: On the dome effect of Eppley pyrgeometers and pyranometers. *Geophys. Res. Letters*, **27(7)**, 971-974.

Jonsson, P, I. Eliasson, B. Holmer and C. S. B. Grimmond, 2006: Longwave incoming radiation in the Tropics: results from field work in three African Cities. *Theor. Appl. Climatol.*, **85**, 185-201.

Karam, H.A., A.J. Pereira-Filho, V. Mason, J. Niolhan, E.P. Marques-Filho, 2009: Formulation of tropical town energy budget (t-TEB) scheme. *Theor. Appl. Climatol*., **100**, 1-10.

Long, C. N., and D. D. Turner, 2008: A method for continuous estimation of clear sky downwelling longwave radiative flux developed using ARM surface measurements. *J. Geophys. Res.*, **113**, D18206.

Lütkepohl, H., 1991: Introduction to multiple time series analysis. Springer Verlag, Berlin, 545 pp.

Malek, E., 1997: Evaluation of effective atmospheric emissivity and parameterization of cloud at local scale. *Atmos. Res.*, **45**, 41-54.

Marciotto, E.R., 2008: Estudo da influência de um dossel urbano sobre o balanço de energia na superfície e implicações na estrutura vertical da camada limite atmosférica. Tese de Doutorado. Departamento de Ciências Atmosféricas, Instituto de Astronomia, Geofísica e Ciências Atmosféricas, Universidade de São Paulo, São Paulo, SP, Brasil, 120 pp. (available in Portuguese at: http://www.iag.usp.br/meteo/labmicro/publicacoes/Teses& Dissertacoes/).

Martilli, A., A. Clappier, M.W. Rotach, 2002: An urban surface exchange parameterization for mesoscale models. *Bound-Layer Meteor.* **104**, 261-304.

Marty, C., R. Philipona, J. Delamere, E. G. Dutton, J. Michalsky, K. Stamnes, R. Storvold, T. Stoffel, S. A. Clough and E. J. Mlawer, 2003: Downward longwave irradiance uncertainty under artic atmospheres: Measurements and modeling. *J. Geophys. Res.*, **108(D12)**, 4358.

Mlakar, P., and M. Božnar, 1997: Perceptron neural network-based model predicts air pollution. In: *Proceedings of Intelligent Information Systems IIS'97*, Ed. H. Adeli. Grand Bahama Island, Bahamas, IEEE Computer society, 345-349.

Mlawer, E. J., S. J. Taubman, P. D. Brown, M. J. Iacono and S. A. Clough, 1997: Radiative transfer for inhomogeneous atmospheres: RRTM, a validated correlated-k model for the longwave. *J. Geophys. Res.*, **102(D14)**, 16 663-16 682.

Nair, K.N., E.D. Freitas, O.R. Sánchez-Ccoyllo, M.A.F. Silva Dias, P.L. Silva Dias, M.F. Andrade, O. Massambani, 2004: Dynamics of urban boundary layer over São Paulo associated with mesoscale processes, *Meteor. Atmos. Phy*s., 86, 87-98.

Niemelä, S., P. Räisänen and H. Savijärvi, 2001: Comparison of surface radiative flux parameterizations Part I: Longwave radiation. *Atmos. Res.,* **58**, 1-18.

Offerle, B., C.S.B. Grimmond, T.R. Oke, 2003: Parameterization of net all-wave radiation for urban areas. *J. Appl. Meteor.* **42**: 1157-1173.

Oliveira, A. P., E. J. Escobedo, A. J. Machado and J. Soares, 2002a: Diurnal evolution of solar radiation at the surface in the City of São Paulo: seasonal variation and modeling. *Theor. Appl. Climatol.,* **71(3-4)**, 231-249.

——, E. J. Escobedo, A. J. Machado, 2002b: A new shadow-ring device for measuring diffuse solar radiation at surface. *J. Atmos. Oceanic Techno.*, **19(5)**, 698-708.

——, R. Bornstein and J. Soares, 2003: Annual and diurnal wind patterns in the city of São Paulo. *Water, Air and Soil Pollution: FOCUS*, **3**, 3-15**.**

——, J. Soares, M. Z. Božnar, P. Mlakar and J. F. Escobedo, 2006: An application of neural technique to correct the dome temperature effects on pyrgeometer measurements. *J. Atmos. Oceanic Technol.,* **23,** 80-89.

Payne, R. E., and S. P. Anderson, 1999: A new look at calibration and use of Eppley precision infrared radiometers. Part II: Calibration and use of the Woods Hole oceanographic institution improved meteorology precision infrared radiometer. *J. Atmos. Oceanic Technol.*, **16**, 739–751.

Pérez, M., and L. Allados-Arboledas, 1998: Effects of natural ventilation and solar radiation on the performance of pyrgeometers. *J. Atmos. Oceanic Technol.*, **16**, 174–180.

Philipona, R., C. Fröhlich and Ch. Betz, 1995: Characterization of pyrgeometers and the accuracy of atmospheric long-wave radiation measurements. *App. Optics,* **34(9)**, 1598-1605.

——, E. G. Dutton, T. Stoffel, J. Michalsky, I. Reda, A. Stifter, P. Wendling, N. Wood, S. A. Clough, E. J. Mlawer, G. Anderson, H. E. Revercomb and T. R. Shippert, 2001: Atmospheric longwave irradiance uncertainty: Pyrgeometers compared to an absolute sky-scanning radiometer, atmospheric emitted radiance interferometer, and radiative transfer model calculations. *J. Geophys. Res.*, **106(D22)**, 28129-28141.

——, B. Dür and C. Marty, 2004: Greenhouse effect and altitude gradients over the Alps – by surface longwave radiation measurements and model calculated LOR. *Theor. Appl. Climatol.*, **77**, 1-7.

Prata, A. J., 1996: A new long-wave formula for estimating downward clear-sky radiation at the surface. *Q.J.R. Meteorol. Soc*., **122**, 1127-1151.

Snedecor, G. W. and Cochran, W. G., 1989: *Statistical Methods, Eighth Edition*. Iowa State University Press. 503 pp.

Soares J., A. P. Oliveira, M. Z. Boznar, P. Mlakar, J. F. Escobedo and A. J. Machado, 2004: Modeling hourly diffuse solar radiation in the city of São Paulo using neural network technique. *Applied Energy*. **79**, 201-14.

Swinbank, W.C., 1963: Long-wave radiation from clear skies. *Q.J.R. Meteorol. Soc.,* **89**, 339-348.

Targino, A. C. L., and J. Soares, 2002: Modeling surface energy fluxes for Iperó, SP, Brazil: An approach using numerical inversion. *Atmos. Res.* **63(1)**, 101-121

Turner, D. D., D. C. Tobin, S. A. Clough, P. D. Brown, R. G. Ellingson, E. J. Mlawer, R. O. Knuteson, H. E. Revercomb, T. R. Shippert, W. L. Smith and M. W. Shephard, 2004: The QME AERI LBLRTM: A closure experiment for downwelling high spectral resolution infrared radiance. *J. Atmos. Sci.*, **61**, 2657-2675.

Wilber, A. C., G. L. Smith, S. K. Gupta and P. W. Stackhouse Jr., 2006: Annual cycles of surface shortwave radiative fluxes. *J. Climate*, **19,** 535-547.

Wilks, D. S., 2006: *Statistical Methods in the Atmospheric Sciences*. International Geophysics Series 2nd, 648 pp.

Willmott, C. J., 1981: On the validation of models. *Physic Geogr.* **2**, 184-194.

——, 1982: Some comments on the evaluation of model performance. *Bull. Amer. Met. Soc.* 1309-1313.

Figure Labels

Fig. 1. Geographic position of the (a) state of São Paulo, (b) city of São Paulo and (c) IAG meteorological station. The *SRB* area is indicated by a white square.

Fig. 2. Time series of raw (a) global solar radiation, (b) air temperature and (c) downward atmospheric longwave radiation at the surface. Time series of filtered (d) global solar radiation, (e) air temperature and (f) downward atmospheric longwave radiation.

Fig. 3. (a) Time variation of the difference between *LW* corrected, prior 15 October 2003 by the NN and after this date by the heat balance equation and (b) dispersion diagram of *LW* obtained from neural network (LW_{NN}) versus *LW* corrected by the heat balance equation ($LW_{CORRECTED}$) for 2004. The vertical bar in (a) indicates October 2003. The gray line in (b) indicates the linear fit between LW_{NN} and $LW_{CORRECTED}$.

Fig. 4. Seasonal variation of monthly-averaged values of *LW* based on observations carried out in São Paulo from 1997-2006 (white columns) and estimated from *SRB* during 1998–2004 (gray columns). The error is given by the vertical bars. The *MBE* (black line) is between observations and *SRB* dataset.

Fig. 5. Time variation of annually-averaged values of *LW* observed at IAG (white columns) during 1997 – 2006 and estimated from *SRB* (gray columns) during 1998–2004. The error is given by the vertical bars. The *MBE* (black line) is between observations and *SRB* dataset.

Fig. 6. Seasonal variation of the diurnal evolution of monthly-averaged hourly values of *LW* (W m^{-2}).

Fig. 7. Seasonal variation of clear sky day frequency in São Paulo, between 1997 and 2006.

Fig. 8. Seasonal variation of monthly averaged values of (a) *LW*, (b) air temperature, (c) air vapor pressure and (d) effective atmospheric emissivity at the surface. The solid circles

indicate all days (all sky conditions) and the open circles indicate clear sky days. The error is given by the vertical bars.

Fig. 9. Diurnal variation of monthly-averaged hourly values of (a) *LW*, (b) air temperature, (c) air vapor pressure and (d) effective atmospheric emissivity at the surface. The solid black circles indicate the monthly-averaged hourly values for August of the entire dataset. The open circles indicate the monthly-averaged values for clear sky day observations for August of the entire dataset. The error is given by the vertical bars.

FIG. 10. Performance of the *LW* expressions and *PEA* in terms of (a) *MBE* (gray column), *RMSE* (white column) and index of agreement, *d* (solid dot), for clear days of the entire period and (b) *MBE* for day (white column) and nighttime (gray column) periods.

FIG. 11. Diurnal variation of effective atmospheric emissivity observed and modeled by *PEA* and Brunt empirical expression estimated using monthly average hourly values of screen air temperature and vapor pressure observed during clear sky days in August of the entire dataset.

Table labels

TABLE 1. Sensors and measurement period.

TABLE 2. Monthly averaged values of *LW*, MBE, number of *LW* data values available in each month and corresponding data fraction. Observation begins on October 1 of 1997 and ends on August 31 of 2006. MBE is estimated with respect to LW_{SRB}.

TABLE 3. Annual averaged values of *LW*, MBE, number of *LW* data values available in each year and corresponding data fraction. Data fraction of the available data corresponding to summer (December, January, February) and winter (June, July, August) periods for each year. Observation begins on October 1 of 1997 and ends on August 31 of 2006. MBE is estimated with respect to LW_{SRB}.

TABLE 4. Empirical expressions used to estimate the downward atmospheric longwave radiation at the surface for clear sky conditions.

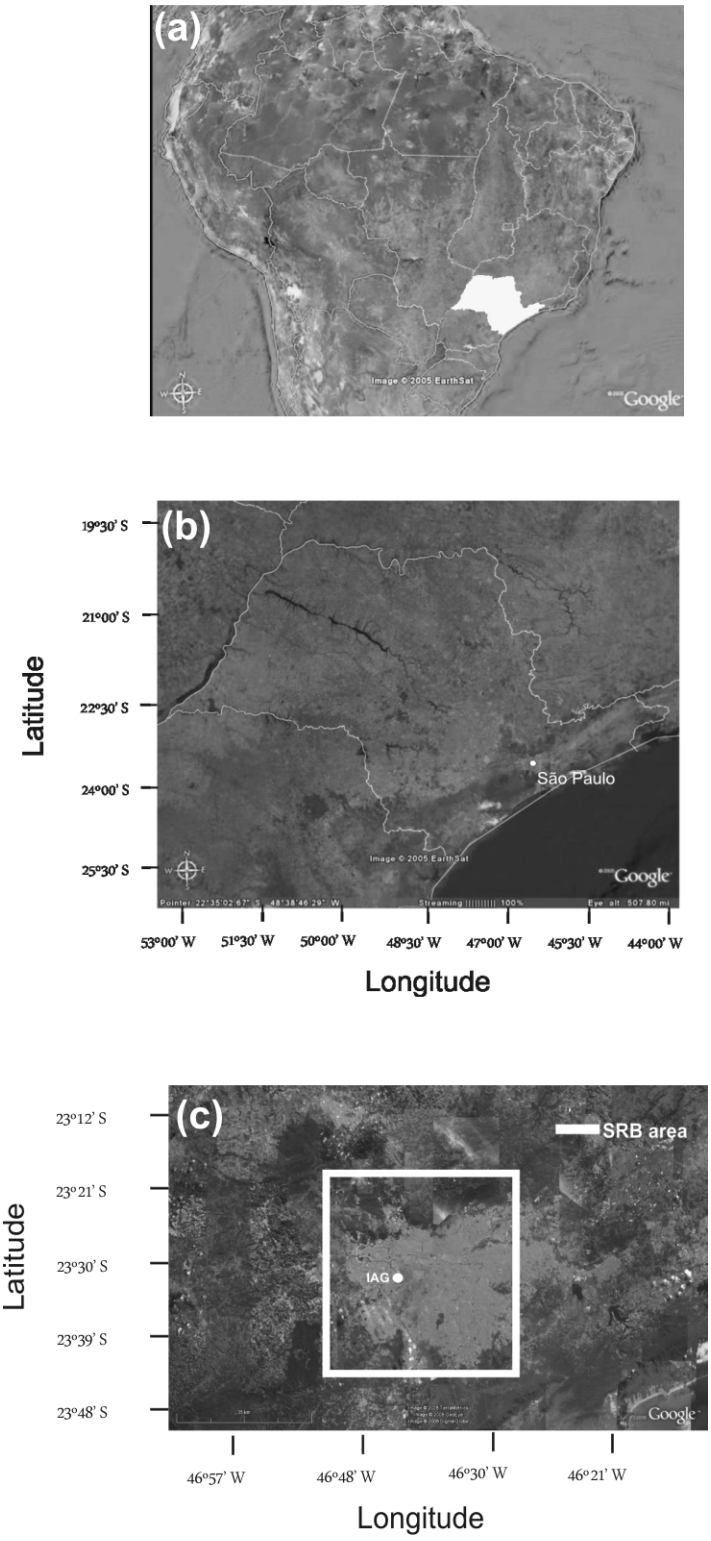

Fig. 1. Geographic position of the (a) state of São Paulo, (b) city of São Paulo and (c) IAG meteorological station. The SRB area is indicated by a white square.

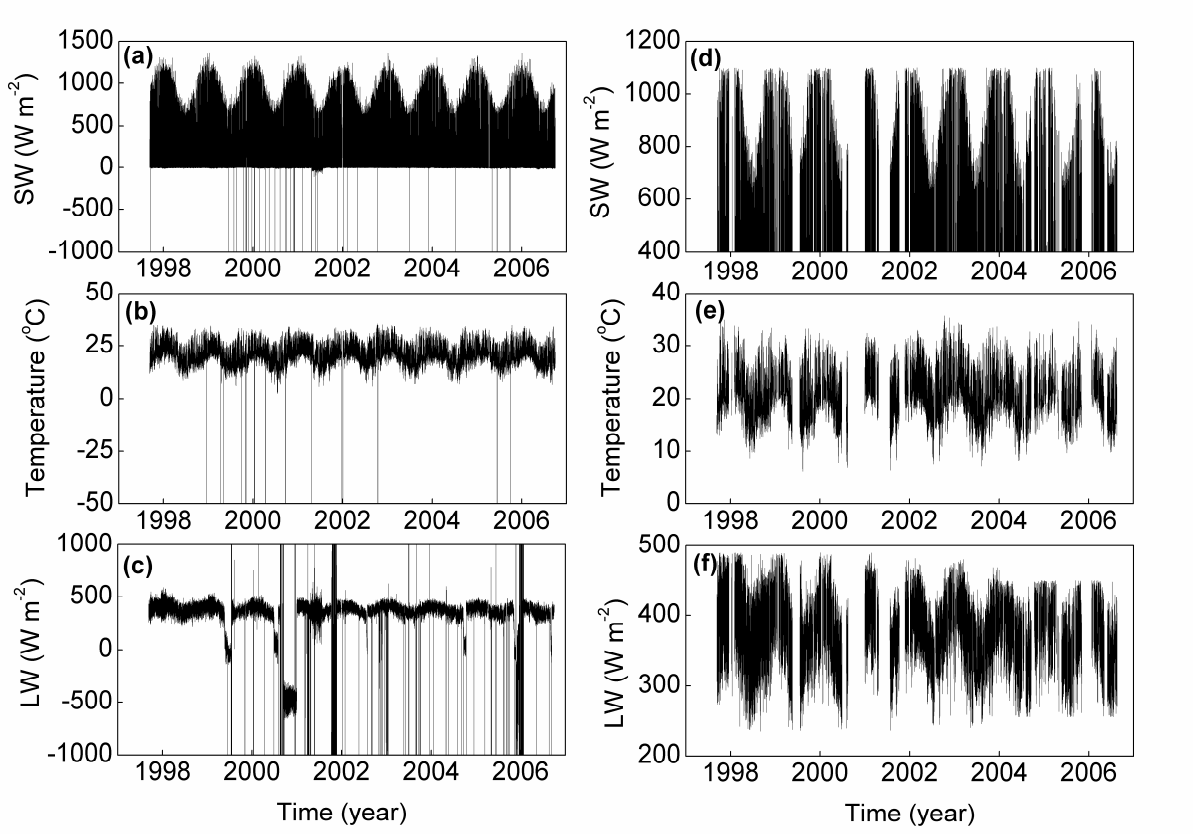

Fig. 2. Time series of raw (a) global solar radiation, (b) air temperature and (c) downward atmospheric longwave radiation at the surface. Time series of filtered (d) global solar radiation, (e) air temperature and (f) downward atmospheric longwave radiation.

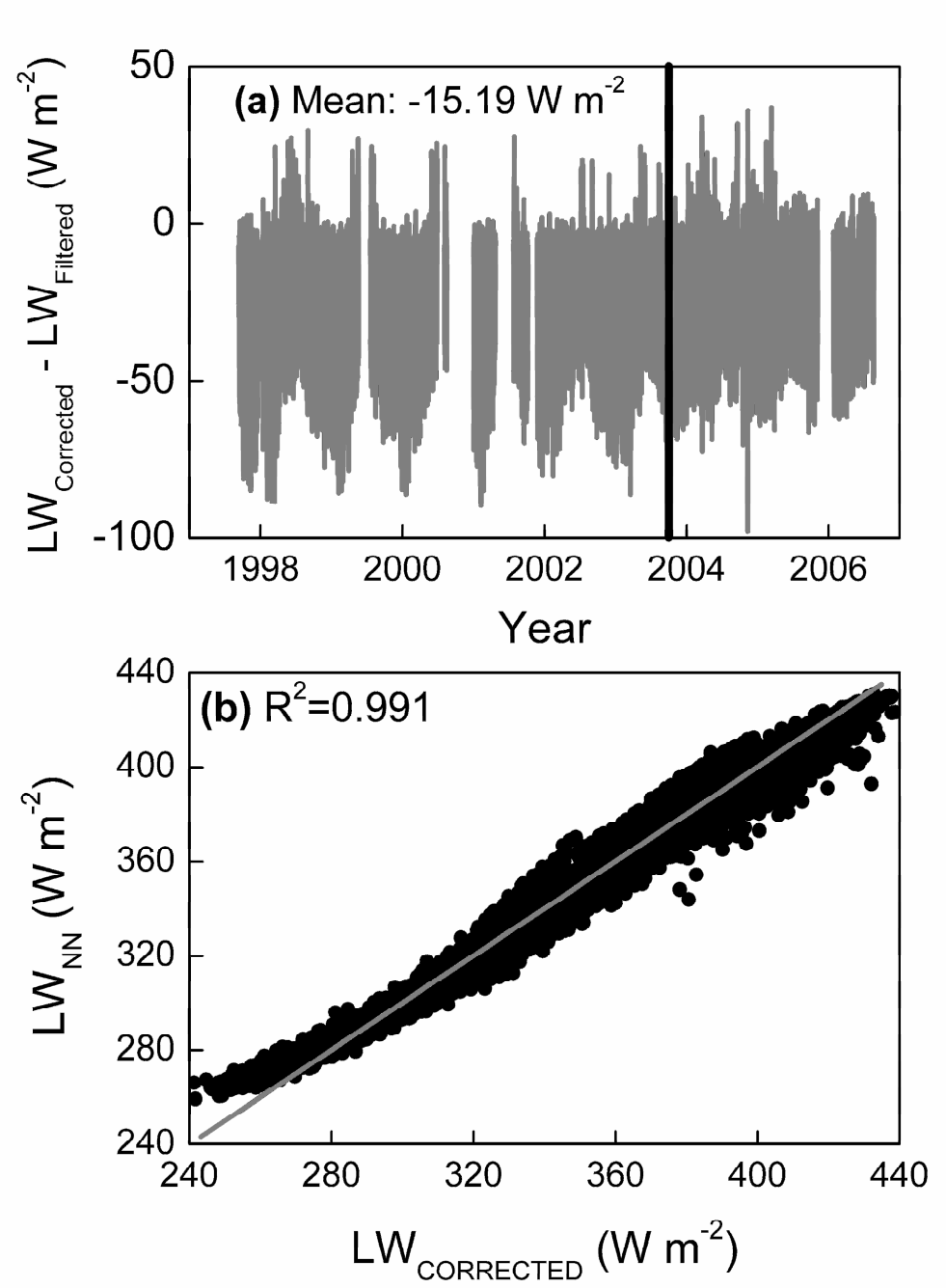

Fig. 3. (a) Time variation of the difference between *LW* corrected, prior 15 October 2003 by the NN and after this date by the heat balance equation and (b) dispersion diagram of *LW* obtained from neural network (LW_{NN}) versus *LW* corrected by the heat balance equation ($LW_{CORRECTED}$) for 2004. The vertical bar in (a) indicates October 2003. The gray line in (b) indicates the linear fit between LW_{NN} and $LW_{CORRECTED}$.

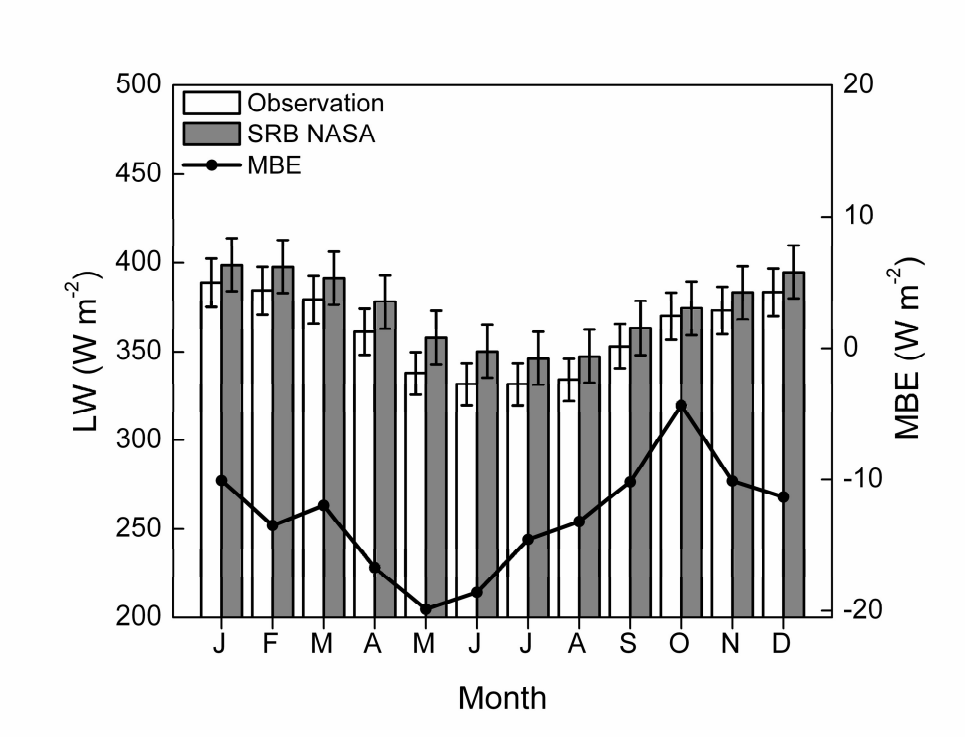

Fig. 4. Seasonal variation of monthly-averaged values of *LW* based on observations carried out in São Paulo from 1997-2006 (white columns) and estimated from *SRB* during 1998–2004 (gray columns). The error is given by the vertical bars. The *MBE* (black line) is between observations and *SRB* dataset.

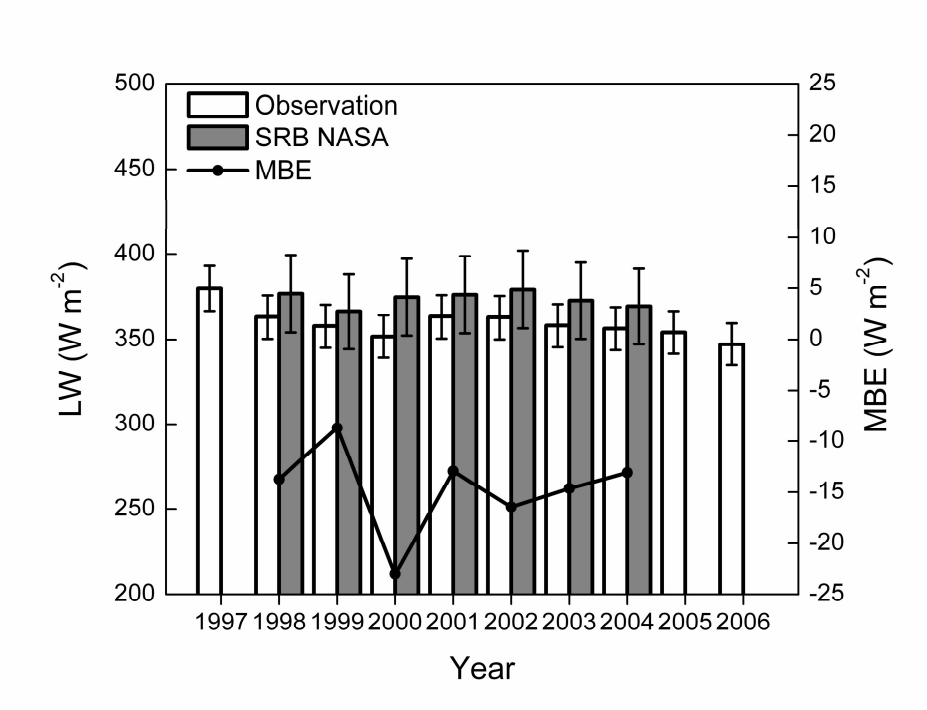

Fig. 5. Time variation of annually-averaged values of *LW* observed at IAG (white columns) during 1997 – 2006 and estimated from *SRB* (gray columns) during 1998–2004. The error is given by the vertical bars. The *MBE* (black line) is between observations and *SRB* dataset.

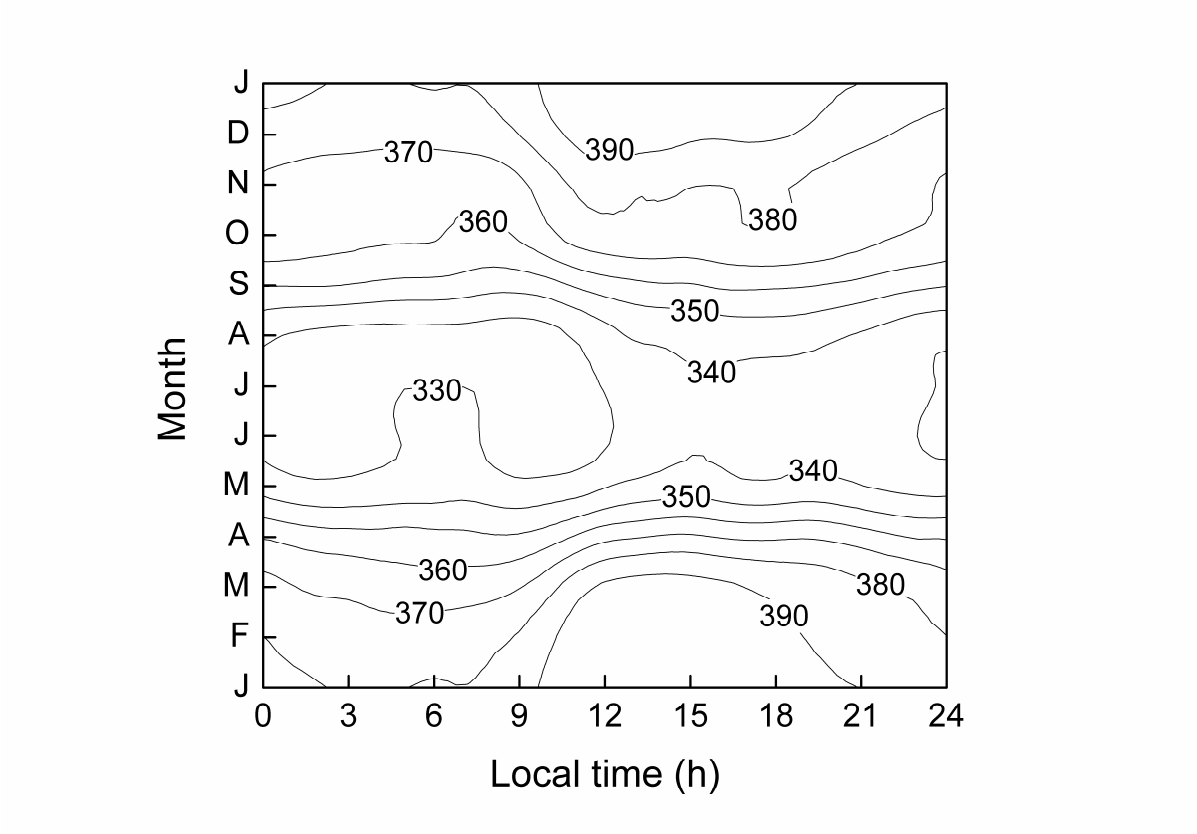

Fig. 6. Seasonal variation of the diurnal evolution of monthly-averaged hourly values of *LW* (Wm^{-2}).

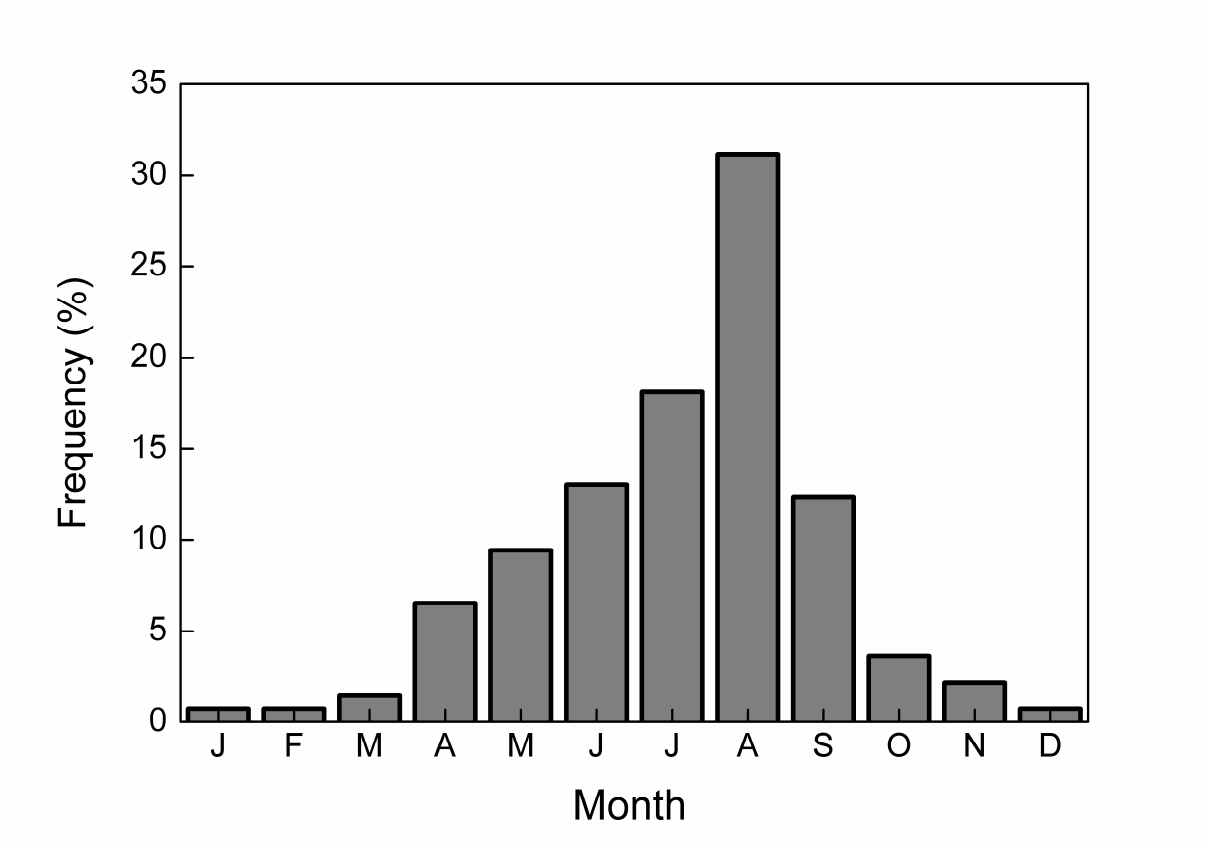

Fig. 7. Seasonal variation of clear sky day frequency in São Paulo, between 1997 and 2006.

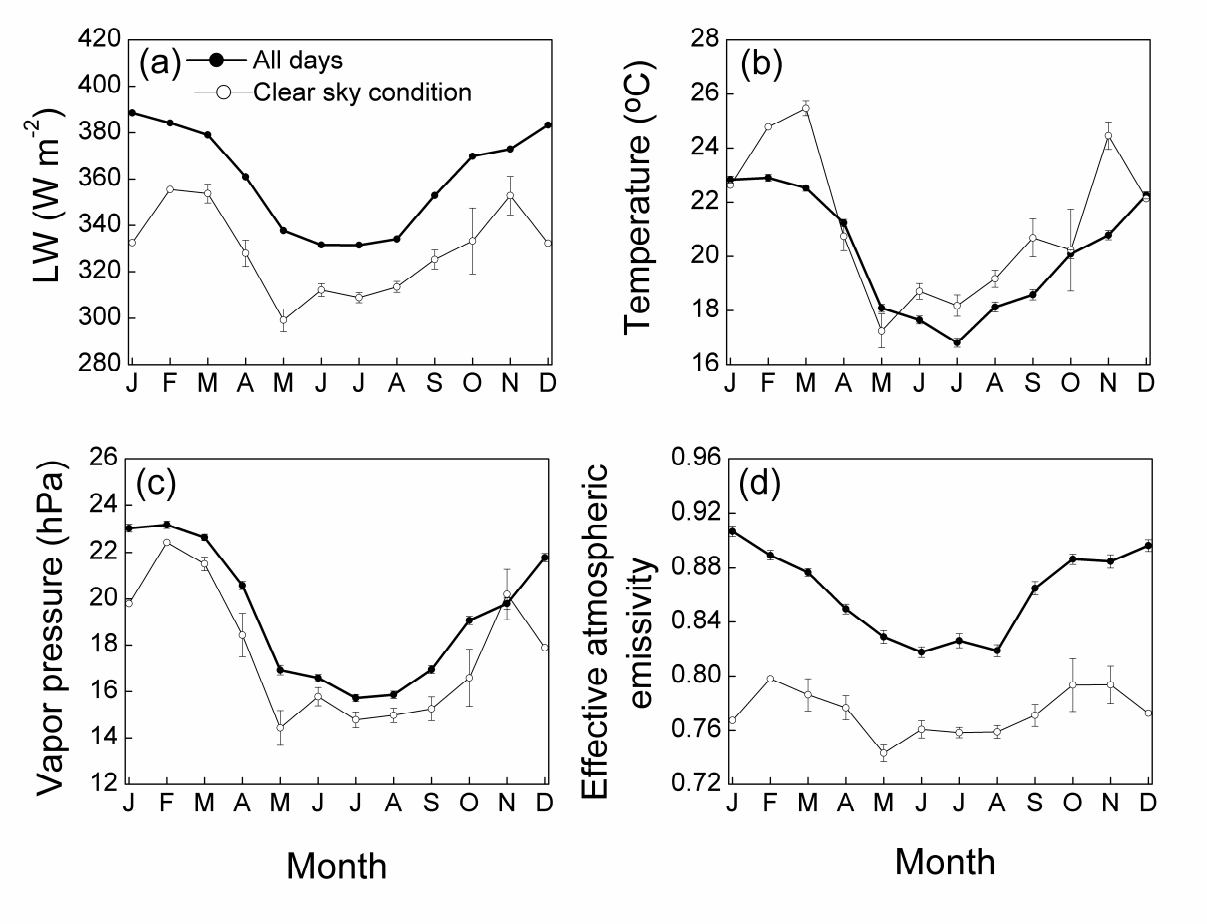

Fig. 8. Seasonal variation of monthly averaged values of (a) *LW*, (b) air temperature, (c) air vapor pressure and (d) effective atmospheric emissivity at the surface. The solid circles indicate all days (all sky conditions) and the open circles indicate clear sky day. The error is given by the vertical bars.

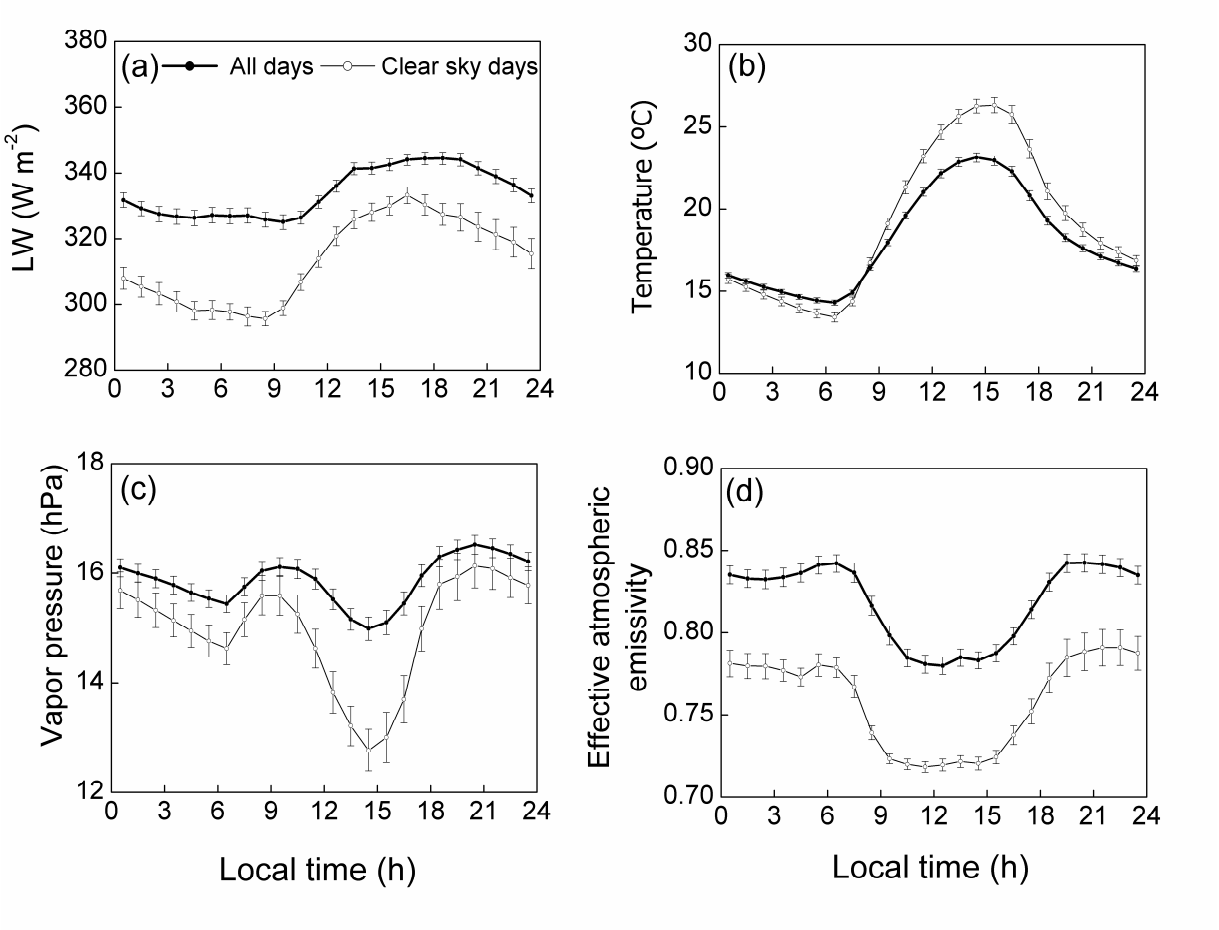

Fig. 9. Diurnal variation of monthly-averaged hourly values of (a) *LW*, (b) air temperature, (c) air vapor pressure and (d) effective atmospheric emissivity at the surface. The solid black circles indicate the monthly-averaged hourly values for August of the entire dataset. The open circles indicate the monthly-averaged values for clear sky day observations for August of the entire dataset. The error is given by the vertical bars.

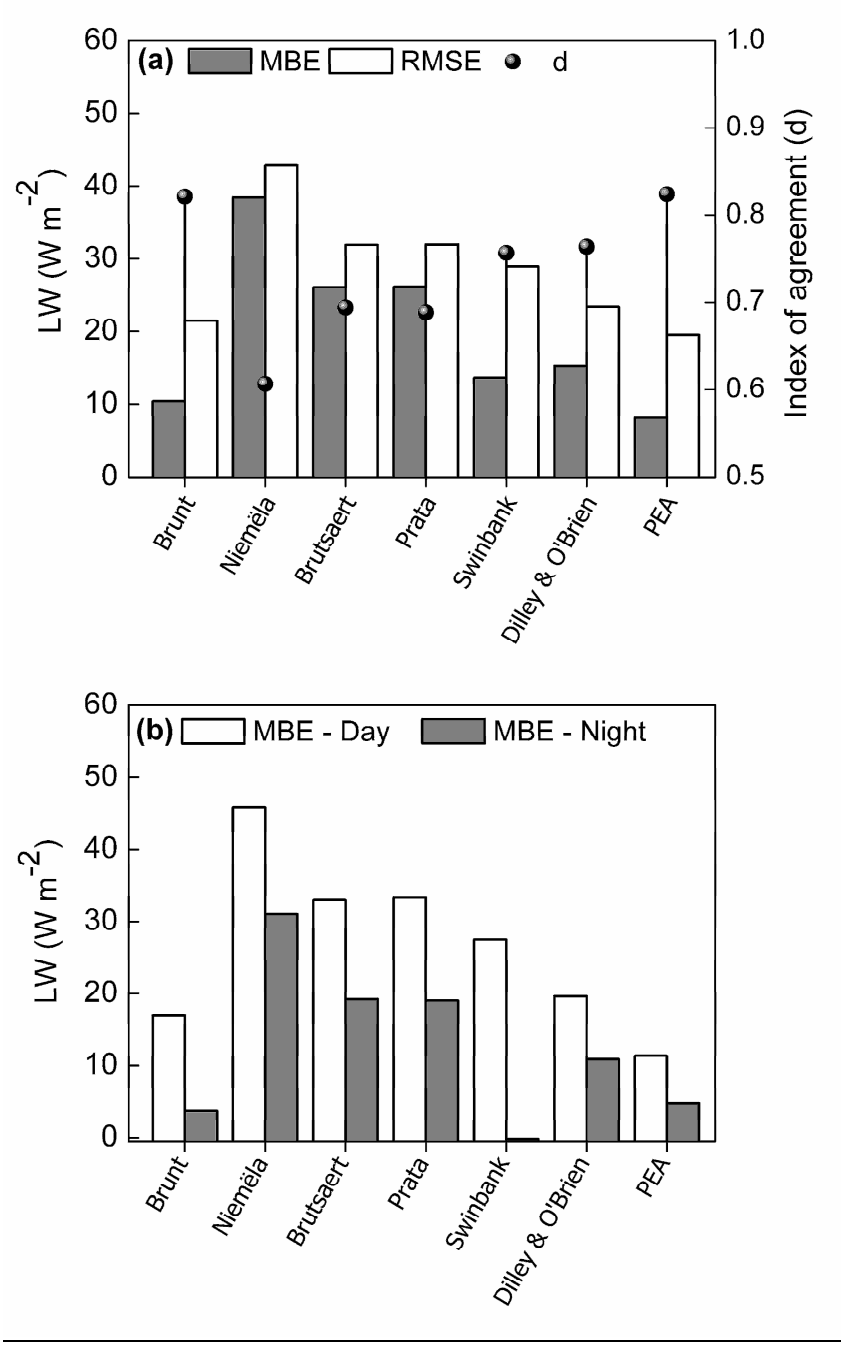

FIG. 10. Performance of the *LW* expressions and *PEA* in terms of (a) *MBE* (gray column), *RMSE* (white column) and index of agreement, *d* (solid dot), for clear days of the entire period and (b) *MBE* for day (white column) and nighttime (gray column) periods.

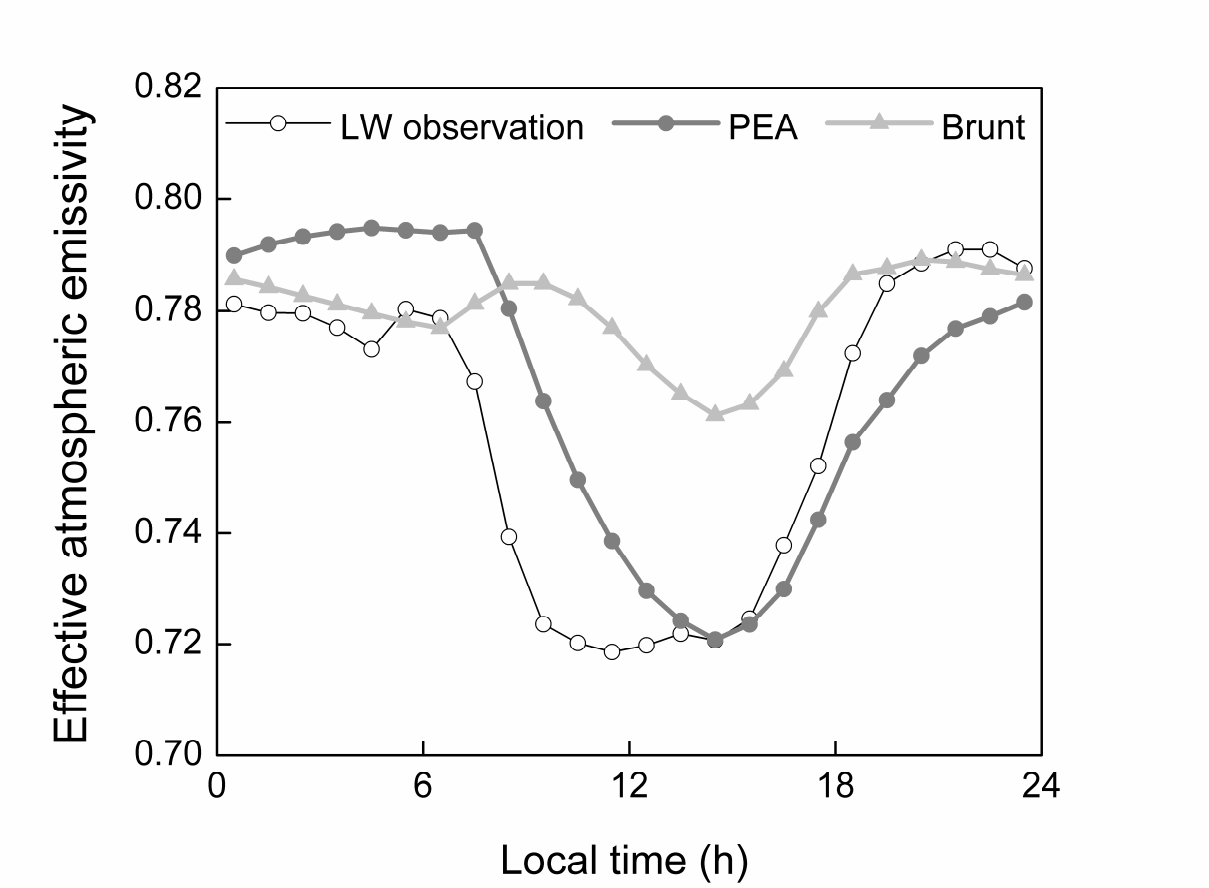

FIG. 11. Diurnal variation of effective atmospheric emissivity observed and modeled by *PEA* and Brunt empirical expression estimated using monthly average hourly values of screen air temperature and vapor pressure observed during clear sky days in August of the entire dataset.

TABLE 1. Sensors and measurement period.		
Variable	**Sensor**	**Period**
Longwave radiation, 5-minutes average	Pyrgeometer, Model PIR, Eppley Lab. Inc.	1997 - 2006
Global solar radiation, 5-minutes average	Pyranometer, Model 8-48, Eppley Lab. Inc.	1997 - 2006
Diffuse solar radiation, 5-minutes average	Pyranometer, Model PSP, Eppley Lab. Inc.	1997 - 2006
Air temperature, 5-minutes average	HMP35C Vaisala	1997 - 2006
Relative humidity, 5-minutes average	HMP35C Vaisala	1997 - 2006
LW, monthly average	Project SRB/NASA	1998 - 2004

TABLE 2. Monthly averaged values of *LW*, MBE, number of *LW* data values available in each month and corresponding data fraction. Observation begins on October 1 of 1997 and ends on August 31 of 2006. MBE is estimated with respect to LW_{SRB}.

Month	LW^{*} (W m^{-2})	*MBE* (W m^{-2})	Number of 5 minute values	Data fraction (%)
January	388.6 ±13.7	-10.1	123	44.1
February	384.2 ±13.6	-13.5	158	62.7
March	379.0 ±13.4	-12.0	228	81.7
April	361.1 ±12.8	-16.7	213	78.9
May	337.8 ±12.0	-19.9	165	59.1
June	331.6 ±11.7	-18.6	192	71.1
July	331.5 ±11.8	-14.6	160	57.3
August	334.1 ±11.8	-13.2	221	79.2
September	352.9 ±12.5	-10.2	183	67.8
October	369.8 ±13.1	-4.3	189	67.7
November	372.9 ±13.2	-10.1	132	48.9
December	383.2 ±13.6	-11.3	129	46.2

(*) *LW* errors were obtained by Gaussian error propagation of statistical and sensor errors.

TABLE 3. Annual averaged values of LW, MBE, number of LW data values available in each year and corresponding data fraction. Data fraction of the available data corresponding to summer (December, January, February) and winter (June, July, August) periods for each year. Observation begins on October 1 of 1997 and ends on August 31 of 2006. MBE is estimated with respect to LW_{SRB}.

Year	*LW** (W m^{-2})	*MBE* (W m^{-2})	Number of 5 minute values	Data fraction (%)	Summer data fraction (%)	Winter data fraction (%)
1997	379.9 ± 13.3	-	23168	22.0	16.6	0
1998	363.0 ±12.7	-13.7	84248	80.1	39.8	97.7
1999	357.7 ±12.5	-8.7	65560	62.4	53.0	44.5
2000	351.6 ±12.3	-23.1	41650	39.6	33.1	41.2
2001	363.2 ±12.7	-13.0	51444	48.9	69.5	40.2
2002	362.7 ±12.7	-16.5	88921	84.6	67.4	91.3
2003	358.0 ±12.5	-14.6	88014	83.7	66.2	92.3
2004	356.3 ±12.5	-13.1	70404	67.0	55.2	69.4
2005	354.1 ±12.4	-	47632	45.3	27.5	71.5
2006	347.2 ±12.2	-	41093	39.1	24.3	73.7

(*) *LW* errors were obtained by Gaussian error propagation of statistical and sensor errors.

TABLE 4. Empirical expressions used to estimate the downward atmospheric longwave radiation at the surface for clear sky conditions.

Author (year)	Expression
Brunt (1932)	$(0.52+0.065\sqrt{e_0})\sigma T_0^4$
Swinbank (1963)	$(9.2\times10^{-6}T_0^2)\sigma T_0^4$
Brutsaert (1975)	$1.24\left(\frac{e_0}{T_0}\right)^{\frac{1}{7}}\sigma T_0^4$
Prata (1996)	$\left\{1-\left(1+46.5\left(\frac{e_0}{T_0}\right)\right)exp\left[-\left(1.2+3\left(46.5\left(\frac{e_0}{T_0}\right)\right)\right)^{\frac{1}{2}}\right]\right\}\sigma T_0^4$
Dilley and O´Brien (1998)	$59.38+113.7\left(\frac{T_0}{273.16}\right)^6+96.96\sqrt{18.6\left(\frac{e_0}{T_0}\right)}$
Niemelä (2001)	$[0.72+0.009(e_0-2)]\sigma T_0^4$

Where e_0, T_0 and σ are respectively the water vapor pressure (hPa), air temperature (K) measured at screen-level and Stefan Boltzmann constant ($5.67\text{x}10^{-8}$ W m^{-2} K^{-4}).